Photorealistic Models for Pupil Light Reflex and Iridal Pattern Deformation

VITOR F. PAMPLONA and MANUEL M. OLIVEIRA
Universidade Federal do Rio Grande do Sul
and
GLADIMIRV.G. BARANOSKI
University of Waterloo
and
SEAN FOGARTY
University of Illinois at Urbana-Champaign

We introduce a physiologically-based model for pupil light reflex (PLR) and an image-based model for iridal pattern deformation. Our PLR model expresses the pupil diameter as a function of the lighting of the environment, and is described by a delay-differential equation, naturally adapting the pupil diameter even to abrupt changes in light conditions. Since the parameters of our PLR model were derived from measured data, it correctly simulates the actual behavior of the human pupil. Another contribution of our work is a model for realistic deformation ofthe iris pattern as a function of pupil dilation and constriction. Our models produce high-fidelity appearance effects and can be used to produce real-time predictive animations of the pupil and iris under variable lighting conditions. We assess the predictability and quality of our simulations through comparisons of modeled results against measured data derived from experiments also described in this work. Combined, our models can bring facial animation to new photorealistic standards. Another contribution of our work is a model for realistic deformation of the iris pattern as a function of pupil dilation and constriction. Another contribution of our work is a model for realistic deformation of the iris pattern as a function of pupil dilation and constriction. Another contribution of our work is a model for realistic deformation of the iris pattern as a function of pupil dilation and constriction.

Categories and Subject Descriptors: • **Information systems→Database management system engines** • **Computing methodologies→Massively parallel and high-performance simulations.** This is just an example, please use the correct category and subject descriptors for your submission. The ACM Computing Classification Scheme:http://www.acm.org/about/class/class/2012. Please read the HOW TO CLASSIFY WORKS USING ACM'S COMPUTING CLASSIFICATION SYSTEM for instructions on how to classify your document using the 2012 ACM Computing Classification System and insert the index terms into your Microsoft Word source file.

Manuel M. Oliveira acknowledges a CNPq-Brazil fellowship (305613/2007-3). Gladimir V G. Baranoski acknowledges a NSERC-Canada grant (238337). Microsoft Brazil provided additional support. Authors' addresses: Sean Fogarty, (Current address) NASA Ames Research Center, Moffett Field, California 94035.

DOI:http://dx.doi.org/10.1145/1559755.1559763

Additional Key Words and Phrases: Face animation, image-based modeling, iris animation, photorealism, physiologically-based modeling

ACM Reference Format:

Vitor F. Pamplona, Manuel M. Oliveira, Gladinir V.G. Baranoski, and Sean Fogarty.2009. Photorealistic models for pupil light reflex and iridal pattern deformation. ACM Trans. Graph.28, 4, Article 106 (September 2009), 8 pages.
DOI:http://dx.doi.org/10.1145/1559755.1559763

1. INTRODUCTION

Arguably, the most important features in facial animation are the eyes, which are essential not only in directing the gaze of the audience [Bahrami et al. 2007], but also in conveying the appropriate degree of expression through pupil dilation and constriction movements. Hence, for animations depicting close-up views of the face, natural-looking eyes and pupil movements are highly desirable.

> "Walt Disney once said to his animation team that the audience watches the eyes and this is where the time and money must be spent if the character is to act convincingly".

Differently from most of the body, the human eye is subject to some involuntary movements of the pupil, which are determined by ambient illumination, drug action, and emotional conditions, among others [Baudisch et al. 2003]. Pupillary light reflex (PLR) is responsible for the constriction of the pupil area in highly lit environments and for its dilation in dimmed ones. PLR is an integral part of our daily experience, and except for drug-induced action, is the single most noticeable of such involuntary movements of the pupil.

The human iris is a muscular tissue containing several easily identifiable structures. Together, they define patterns that are deformed as a result of changes in the pupil diameter. Although pupil light reflex and iridal deformations could be animated using standard computer graphics techniques, which in turn, may result in more realistic and reproducible of these movements.

In this article, we present a physiologically-based model for realistic animation of PLR. Our model combines and extends some theoretical results from the field of mathematical biology [Cole et al. 2006] with experimental data collected by several researchers relating pupil diameter to the intensity of environmental light [Collewign et

al. 1988]. The resulting model produces high- fidelity appearance effects and can be used to produce real-time predictive animations of the pupil and iris under variable lighting conditions (Section 5.4). We model the iridal pattern deformation process by acquiring a set of high-resolution photographs of real irises at different levels of pupillary dilation and by tracking their features across the set of images. By analyzing the tracked positions, we obtained a simple analytical expression for the iridal deformation pattern as a function of the pupil diameter (Section 6). To the best our knowledge, ours is the first physiologically-based model for simulating pupil light reflex presented in the graphics literature (the first model ever to simulate individual variability in terms of PLR sensitivity—Section 5.3), as well as the first model for iridal pattern deformation. Moreover, ours are the first practical models (providing actual coefficient values) in the literature for simulating the dynamics of the pupil and iris under variable lighting conditions. We demonstrate the effectiveness of our approach by comparing the results predicted by our models against photographs and videos captured from real human irises (Figures 1 and 9). Table I summarizes the main mathematical and physical quantities used in the derivation of the proposed models and which are considered throughout this work.

2. RELATED WORK IN COMPUTER GRAPHICS

A few researchers have addressed the issue of realistic human iris synthesis. Lefohn et al. blend several textures created by an artist,each containing some eye feature. Other image-based approaches have been proposed by Cui et al., Wecker et al., and Makthal and Ross. Essentially, they decompose a set of iris images using techniques such as principal component analysis, multiresolution and wavelets, and Markov random fields, and recombine the obtained data to generate new images of irises. Zuo and Schmid created a fiber-based 3D model of the iris. Lam and Baranoski introduced a predictive light transport model for the human iris, which computes the spectral responses of iridal tissues described by biophysical parameters. Francois et al. estimate iris height maps from gray-scale images. All these approaches use stationary pupil sizes.

Sagar et al. developed an anatomically detailed model of the eye to be used in a surgical simulator. In their model, Gaussian perturbations were used to simulate the waviness of ciliary fibers and the retraction of pupillary fibers during pupil dilation. Alternatively, depending on the level of object manipulation, a texture mapping approach was used to model the iridal appearance. It is worth noting, however, that their goal was to achieve functional realism [De- Carlo and Santella 2002] as opposed to physical or photorealism.

3. BRIEF OVERVIEW OF THE HUMAN IRIS AND PUPIL

The human iris has a diameter of about 12 mm and forms a disc that controls how much light reaches the retina. Under high levels of lighting, the iris dilates, flattening itself and decreasing the pupil size. Under low levels of illumination, it constricts, folding itself and increasing the pupil area. The pupil diameter varies from 1.5 mm to 8 mm on average, and in general, it is not a perfect circle. Also, its center may deviate from the center of the iris by an offset of up to 20%. According to Newsome and Loewenfeld, there are no observable differences in the iris regarding light-induced or drug-induced pupil dilation/constriction.

The human iris is divided in two zones by the *collarette,* a delicate zig-zag line also known as the iris frill. The *pupillary* zone is bounded by the pupil, while the *ciliary* zone extends to the outer border of the iris. Each zone is characterized by a muscle. The *sphincter,* located in the pupillary zone, is a concentric muscle that constricts to decrease the pupil size. The *dilator,* found in the ciliary zone, is a radial muscle that constricts to increase the pupil size. These two muscles overlap at the collarette.

The sphincter and dilator muscles are independently connected to the autonomous nervous system (ANS) and the pupil size results from a balance of the separately incoming stimuli to the two muscles [Dodge 1900]. The ANS conducts the pupillary light reflex and *hippus* neural actions. Hippus are spontaneously irregular variations in pupil diameter, which can essentially be characterized as random noise in the 0.05 to 0.3 Hz frequency range. In PLR, when light reaches the retina, neural signals are sent to the brain, which sends back a signal for closing or opening the pupil. Thus, PLR can be modeled in two phases: perception, and after some time delay, adjustment.

4. MODELS OF PUPIL DYNAMICS

The pupillometry literature describes several models built around experiments designed to measure the values of some parameters as a function of incident light intensity. Link and Stark performed a study where a light source was placed in front of the subjects' irises and, by varying the intensity and frequency of the light, they measured the pupillary latency (the time delay between the instant in which the light pulse reaches the retina and the beginning of iridal reaction):

$$\tau(\mathrm{R},\mathrm{L}_{fL}) = 253 - 14\ln(\mathrm{L}_{fL}) + 70R - 29R\ln(\mathrm{L}_{fL}), \qquad (1)$$

where τ is the latency in milliseconds, L_{fL} is the luminance measured in foot-Lamberts (fL), and R is the light frequency measured in Hz.

Other similar models predict an average pupil size as a function of the light intensity using a few experimental measurements [Dodge and Cline 1901]. Among those, the most popular one is the Moon and Spencer model, which is expressed as:

$$D = 4.9 - tanh[0.4(log_{10}(L_b) - 0.5)] \qquad (2)$$

where the pupil diameter, D, varies from 2 to 8 mm, and L_b is the background luminance level expressed in blondels, varying from 10^5 blondels in sunny days to 10^{-5} blondels in dark nights. $\tanh$ is the hyperbolic tangent.

4.1 Physiologically-Based Models

In Mathematical Biology and related fields, models based on physiological and anatomical observations were derived to express the relationships among the pupillary action variables without relying on quantitative experimental data. For example, Usui and Stark proposed a parametric model of the iris to describe the static characteristics of pupil response to light stimuli, and to explain its random fluctuations in terms of probability density functions. Recently, Tilmant et al. proposed a model of PLR based on physiological knowledge and guided by experiments. Although they have obtained plausible results, Tilmant et al. have recommended the use of another physiologically-based model to more accurately monitor pupillary dynamics, namely the time-dependent model developed by Longtin and Milton.

Table I. Summary of the Main Mathematical and Physical Quantities Considered in the Development of the Proposed Models

Symbol	Description	Physical Unit
L_b	Luminance	blondels (B)
L_{fL}	Luminance	foot-Lambert (fL)
I	Illuminance	lumens/mm^2 (lm/mm^2)
R	light frequency	Hertz (Hz)
D	pupil diameter	millimeters (mm)
A	pupil area	square millimeters (mm^2)
r_I	individual variability index	$r_I \varepsilon$ [0,1]
T	current simulation time	milliseconds *(ms)*
τ	pupil latency	milliseconds (ms)
x	muscular activity	none
ρ_i	ratio describing the relative position	none
β, α, γ, k	constants of proportionality	none

This is an example of table footnote. This is an example of table footnote. This is an example of table footnote. This is an example of table footnote. This is an example of table footnote.

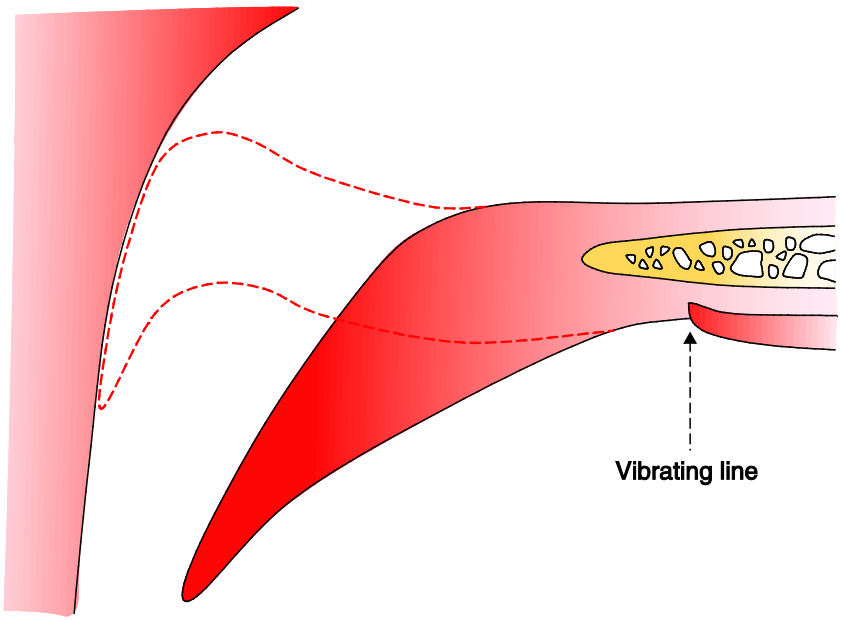

Fig. 1.Comparison of the results predicted by our models against video of a human iris. (left) One frame of an animation simulating the changes in pupil diameter and iridal pattern deformation. (center) One frame from a video of a human iris. (right) Graph comparing the measured pupil diameters from each individual frame of a nine-second-long video sequence (green line) against the behavior predicted by our model (red line). The gray bars indicate the periods in which the light was kept on and off. The complete video sequence and corresponding animation are shown in the accompanying video.

5. THE PROPOSED PHYSIOLOGICAL-BASED MODEL

The model of Moon and Spencer (Equation (2)) is based on a set of discrete measurements and approximates the response on an average individual under various lighting conditions. Their measurements were made after the pupil size had stabilized for each illumination level, and therefore, their model does not describe the pupil behavior outside the equilibrium state. Moreover, pupil size, latency, constriction, and redilation velocities tend to vary among individuals exposed to the same lighting stimulus [Gajewski et al. 2005].

Longtin and Milton's model (Equation (7)) is time dependent and adaptive, with the potential to handle abrupt lighting changes. It is a theoretical model, and unfortunately, Longtin and Milton did not provide the values for the various parameters in their model (i.e., γ, α, θ, n, ϕ), as these, in principle, depend on the abstract notion of iridal muscular activity x, as well as on the use ofthe Hill function. The use of incorrect parameter values will not produce realistic results and may cause Equation (7) to not converge.

5.1 Equilibrium Case

From Equation (2), we can estimate the value of the parameter γ. One should note that L_b is expressed in blondels while ϕ is given in lumens. Although, in general one cannot convert between two pho-

tometric quantities, this can be done under some well-defined situations. Since Moon and Spencer's data were collected with the subject seated before a large white screen of uniform intensity which covers most of their field of view, we assume that the light reaching a person's pupil has been reflected by a perfect (Lambertian) diffuse surface. Recall that an ideal (lossless) diffuse reflector returns all of the incident flux so that its reflectance$\rho = 1$ and its BRDF $f = 1/\pi$. For such a reflector, 1 blondel = 10^{-6} lumens/mm^2.

5.2 The Dynamic Case

Equation (15) cannot be used to describe the evolution of the pupil diameter in time as a function of instantaneous variations of the light intensity arriving at the pupil. Nevertheless, the obtained constants are still valid for the dynamic case, since the equilibrium is just a special case of the more general pupil behavior, for which the constants should also hold.

In general, one cannot take an equation obtained for equilibrium and generalize it to the dynamic case. In our model, however, this is possible because of the following constraints:

(1) g(A) and M(D) have no explicit time dependence;

(2) the range of values assumed by A (or D) is the same for both the equilibrium and the nonequilibrium cases;

(3) there is a one-to-one mapping between A and D.

where T_c and T_p are respectively the current and previous simulation times (times since the simulation started) measured in milliseconds, S is a constant that affects the constriction/dilation velocity and varies among individuals. The higher the S value, the smaller the time step used in the simulation and, consequently, the smaller the pupil constriction/dilation velocity.

Figure 4 shows pupil diameter values corresponding to Moon and Spencer's average subject simulated using Equation (16) considering some abrupt changes in the environment luminance. For this example, our results are compared to results provided by the static models of Moon and Spencer (Equation (2)) and of De Groot and Gebhard.

5.3 Modeling Individual Differences

While Equation (16) simulates dynamic pupil behavior, it only does so for the average individual represented by the Moon and Spencer model. There are, however, substantial differences in the way pupils from different individuals react to a given light stimulus. Such variations include differences in diameter [Google Inc.], latency, and constriction and redilation velocities. In order to simulate individual differences, we cannot just arbitrarily change the parameter values of our model, as Equation (16) may not converge.

Although our model properly simulates the elastic behavior of the iris muscular activity during changes in lighting conditions, it does not model hippus (Equation 16 will converge to some pupil diameter value if the lighting conditions remain constant). As random fluctuations whose causes are still unknown, it is currently not possible to define a physiologically-based model for hippus. We visually approximate the hippus effect by adding small random variations to the light intensity (between $-10^{0.3}$ and $10^{0.3}$ blondels), to induce small variations in the pupil diameter (of the order of 0.2 mm), in the frequency range of 0.05Hz to 0.3Hz.

5.4 The PLR Model Validation

In order to validate our PLR model under nonequilibrium conditions and to show that it is capable of representing individual variability, we performed some qualitative comparisons between actual pupil behavior and the results of simulations produced by our model. For this, we captured videos of normal subjects presenting significantly different light sensitivities (different PLR responses), while a light was turned on and off several times. Since pupil constriction is bigger when both eyes are stimulated, the subjects kept both eyes opened. To avoid fatigue and habituation of the iris, in each experiment we recorded less than one minute of video per subject.

— The image texel size of surface textures that represent 3D elements (e.g. forest) should vary with distance, but should not match true perspective *(texel size* in Section 3.2, Texture Gradients).

— The image space distribution of texel elements of 3D textures (e.g. forest) should mimic one that would result from the projection of homogeneously distributed surface elements *(texel density* in Section 3.2, Texture Gradients).

— Image space texel spacing of 3D textures should ensure that texels overlap, especially in steep areas *(texel occlusion* in Section 3.2, Texture Gradients).

— Fall lines follow essential structures of terrain. They act as surface contours, and are used by panorama artists to paint cliff and snow textures *(fall lines* in Section 3.2, Surface Contours).

— Fall lines are used as imaginary lines along which tree strokes are placed, acting as texture *meta-strokes (meta-strokes* in Section 3.2, Surface Contours).

— Shading tone should have a good distribution of light, medium,and dark values *(shading* in Section 3.2, Shading). —Light position should be placed so that the rendering of the terrain exhibits a good balance of light and shade, as seen from the selected viewpoint *(light direction* in Section 3.2, Shading). —For extended terrain areas, indicating silhouettes, especially between occluding hills, is useful *(silhouettes* in Section 3.2, Silhouettes).

— Water surfaces should reflect the environment *(water textures* in

— Section 3.3, Brushstroke Colors).

— Geometry should be emphasized by use of vertical exaggeration *(vertical exaggeration* in Section 3.4).

We computed the pupil diameters of the subjects at each frame of the video sequences. Lighting measurements made during video capture were used as input to our PLR model for simulating pupil behavior. The pupil diameters resulting from these simulations were then compared to the pupil diameters computed at individual video frames. Note that the simulated results are not expected to quantitatively match the observed ones, but rather be in qualitative agreement with observed behavior.

The videos were captured using a Cannon ELURA2 miniDV camcorder (NTSC, 720X576 pixels) with progressive scan, connected to a PC through a firewire connection. We kept the room's light dimmed so that the subjects' pupils could dilate naturally to some extent, but not so dark that we could not see the pupils in the individual video frames. Because of these constraints, we used two subjects (both males) with light eyes (a 24-year-old with green eyes, and a 26-year-old with blue eyes). For each frame, the pupil diameters were estimated from the set of dark pixels (pupil area P_{area}) inside a specified rectangle containing solely the subject's pupil and part of the iris (Figure 5). Given P_{area}, the pupil diameter was obtained (assuming

the pupil is a circle) as $d = 2\left(\sqrt{P_{area}/\pi}\right)$pixels. The conversion from pixels to millimeters was performed considering a typical iris diameter of 12mm. According to our experience, computing the pupil diameter as described produces more accurate results than computing it as the number of pixels in the largest straight segment in the set of dark pixels (the pupil).

Since the video frames were captured at approximately 30Hz, in practice no variation is expected between the pupil diameters in neighbor frames under constant illumination, even in the presence of hippus. Thus, we estimated the average error in the computed pupil diameters to be approximately 0.1mm by computing the average difference between estimated pupil diameters for neighbor frames. Based on the video sequences, we set $S = 600$ (Equation (16)) for the two subjects in all experiments, as this value made their simulated constriction velocities approximate the ones in the video sequences. We empirically set the frequency of the two light sources used in our experiments to$R = 0.4$Hz, a value that made the latency estimated by Equation (1) approximate the latency observed in the video frames.

To evaluate the quality of our simulations, we performed experiments with both subjects using two different kinds of light sources to induce pupil constriction: a small flashlight and a 100-watt incandescent white light bulb. For light measurements, we used an LD-200 Instrutemp digital lux meter (precision ±3%, frequency 2 Hz).

5.4.1 *The Flashlight Experiments.* In these experiments, we used a light source to induce significant changes in the subjects' pupil diameters without introducing considerable changes in the lighting conditions of the environment. For this purpose, we used a small flashlight powered by a single AAA battery (1.5 Volt) kept at about 20cm from the subject's right eye and pointed at it. Given the small area illuminated by the flashlight as well as its reduced power, the readings from the lux meter were very sensitive to even small changes in the relative position and orientation of the flashlight with respect to lux meter sensor. Thus, we decided to run two simulations using the recorded data: (1) considering the light intensity estimated using Equation (2), and (2) considering the readings from the lux meter. These two experiments are explained next.

In this experiment, we used the Moon and Spencer equation (Equation (2)) to solve for the light intensities during the on and off states of the flashlight, based on the measured pupil diameters (from the video). Since the Moon and Spencer function (curve C_m in Figure 3) represents the pupil behavior of an average individual, we estimated the on (off) light intensity as the average of the computed on (off) intensities for both subjects. Using this procedure, we obtained estimates of $10^{1.1}$ blondels when the flashlight was on, and $10^{-0.5}$ blondels when the flashlight was off. Given the average luminance value for the on (off) state and the corresponding pupil diameter for a given subject, we used Equation (19) to estimate the r_{Ion} (r_{Ioff}) index for that subject. The subject's final r_I index was computed as the average between his r_{Ion} and r_{Ioff} indices. Using this procedure, we obtained $r_I = 0.4$ for the green-eye subject and $r_I = 0.03$ for the blue-eye subject.

Figure 6 shows the actual pupil diameter measurements performed on a frame-by-frame basis along 9-second-long sequences captured for each subject. The green "+" marks on top represent the measurements for the green-eye subject, while the blue "x" marks show the measurements of the blue-eye subject. This example illustrates the intersubject variability in terms of light sensitivity and shows the ability of our model to appropriately represent such individual differences. The vertical dotted lines delimit the intervals in which the flashlight was kept on and off for each subject. The solid and dashed lines represent the simulated results produced by our model for the green-eye and blue-eye subjects, respectively, and closely agree with the actual measured values. These curves were produced automatically from Equations (16) and (19), on top of which we added small random variations (hippus effect) as described in the previous section.

5.4.1.1 *The second flashlight experiment.* In this experiment, we used the readings provided by the lux meter for the on and off states of the flashlight. These illuminance values were 350lux[1] and 90lux, respectively. One should recall that in such a setup, small changes in the position and orientation of the subject's head produce changes in the illuminance at the pupil. Therefore, these values are only approximations to the actual illuminance reaching each subject's lit eye. Given the illuminance values and the subjects' corresponding pupil diameters estimated from the video frames, we obtained the actual pupil's luminous flux (in lumens) at the two flashlight states, for each individual. These values were then converted to blondels according to the assumption described in Section 5.1. We then used Equations (16) and (19) to estimate their corresponding r_I indices (by averaging r_{Ion} and r_{Ioff}), obtaining $r_I = 0.54$ for the blue-eye subject and $r_I = 0.92$ for the green-eye subject. Figure 7 compares the actual pupil measurements (same as in Figure 6) with the results simulated by our model using the lux meter readings as input. The differences between the simulated curves shown in Figures 6 and 7 are primarily due to the added random noise (hippus).

5.4.2 *The 100-Watt Lightbulb Experiment.* For this experiment we used a more stable light source to induce pupil constriction: a spot with a 100-watt incandescent white lightbulb, kept at about one meter in front and one meter to the right of the subject's head. This setup allowed the subjects to remain comfortable with their eyes opened while the light was on.

We measured the environment light intensity during the on and off states by positioning the digital lux meter at approximately the same position and orientation as the subject's right eye. During the blue-eye subject experiment, we found the illuminance to be equal to 140 lux when the light was off and 315 lux when it was on. During the green-eye subject experiment, the readings were 91 and 540 lux, respectively. These differences resulted from a darker environment and a slight approximation of the green-eye subject to the light source. Again, we used the illuminance values and the subjects' corresponding pupil diameters (measured from the video) as input to Equations (16) and (19) to estimate their corresponding r_I indices (by averaging r_{Ion} and r_{Ioff}). We obtained $r_I = 0.9$ for the blue-eye subject and $r_I = 1.0$ for the green-eye subject.

Figure 8 (top) shows the actual pupil diameter measurements performed on a frame-by-frame basis along 56- and 50-second- long sequences captured for the blue-eye and for the green-eye subjects, respectively. The vertical lines delimit the intervals in which the light was kept on and off for each subject. The solid and dashed lines represent the simulated results produced automatically by our model (Equations 16 and 19) with and without hippus, respectively, and closely agree with the actual measurements. Figure 8 (bottom) shows zoomed versions of portions of the graphs shown on top, exhibiting off-on-off transitions.

An important point to note is that by using an average of the estimated r_I indices for the on and off states of the light source, ourmodel is capable of realistically simulating the pupil behavior of individuals with considerable differences in PLR responses under different and variable lighting conditions.

[1] 1 lux = 1 lumen/m^2.

6. MODELING THE IRIS DEFORMATION

Although the iris is a well-known structure, there is no general agreement about a model of its behavior. He suggested that the collagen fibers are arranged in a series of parallel arcs, connecting the iris root with the pupil border, clockwise and counterclockwise in an angle of 90 degrees oriented by the center of the pupil. These fibers would be interwoven with other iris components, such as blood vessels. Based on Rohen's fiber arrangement, Wyatt proposed a 2D nonlinear model for iris deformation. Such a model has been validated on canine, porcine, and monkey irises, but so far not on human irises [Wyatt private communication].

Figure 9 (right) shows how the positions of the individually tracked iridal feature points changed along the dilation process. The trajectories of the points both on the pupillary and ciliary zones move on approximately radial paths. Although some imprecision in the exact location of the points might have resulted from the manual specification, most of the deviation from the radial paths result from the existence of blood vessels under the iris, and from crypts, and folds (the iris folds its tissue as a result of pupil dilation) that prevent iris points from always moving along radial lines. Such structures vary considerably among individuals but, according to our experience, their influence on the paths of the feature points usually has small magnitude (Figure 9 right). Therefore, as a first approximation, we can assume that the iris points move along straight lines in the radial directions. It is worth noting that Wyatt's 2D model does not take the influence of these structures into account either.

6.1 Animating the Deformed Iridal Patterns

As an approximation to the behaviors depicted in Figures 9 (right) and 10 (right), we use texture mapping to animate the iris deformation process. Note that this is a natural and efficient way of implementing the behavior modeled by Equation (20): as the pupil dilates/constricts, the iris ring is compressed/stretched, but the parameterization (in the [0,1] x [0,1] domain) of the points inside the ring remains the same. Thus, for animation purposes, we model the iris as a planar triangle-strip mesh on the disk defined by the two circles with a small pupil diameter as a texture. Texture coordinates map the border of the pupil to the inner circle of the mesh, and outer border of the iris to the mesh's outer circle. Currently, we tessellate the mesh creating a pair of triangles at every five degrees. The animation proceeds by computing the new pupil diameter D as a function of the incident lighting using Equation (19). We then reposition each vertex v_i, located on the inner circle of the mesh, at a distance D/2 along the radial line connecting the center of the pupil to v_i, while keeping their original texture coordinates unchanged. One should recall that the center of the pupil does not necessarily match the center of the iris, and thus, it is important to keep the coordinates of the center of the pupil. Figure 8 shows the renderings of an iris created using our models for different lighting conditions. Note that the patterns deform in a natural way. No light reflection on a corneal surface has been simulated, to avoid masking iris details.

7. DISCUSSION

We have implemented the proposed models and used them to render synthetic images of the human iris and pupil. The resulting animations are very convincing and run in real time. We have compared the images produced by our models with photographs and videos of real human irises. The results produced by our models are in qualitative agreement with observed behavior in humans.

Accommodation and age affect the pupil diameter and iris color influences some PLR parameters, such as maximum pupil diameter, latency, and constriction velocity. These aspects are currently not taken into account by our model because of the lack of reliable data over a large range of lighting conditions. For instance, discuss the effect of age on the size of the pupil. Their study, however, only considered luminance values from 10^1 to 10^4 blondels, which corresponds to only about 30% of the luminance range used by our model. Currently, we model variations in pupil diameters for the same light stimulus using Equation 19, which can be used to simulate the age-related miosis effect reported by Winn. Also, since our model covers the entire range of valid pupil diameter values, it safely covers the pupillary sizes resulting from influence of attentional and other cognitive factors. Extending our model to handle other phenomena based on biophysical parameters is an interesting direction for future work.

8. CONCLUSION

To the best of our knowledge, ours is the first physiologically-based model for simulating pupil light reflex presented in the graphics literature. It is also the first practical model (providing actual coefficient values) in the literature for simulating the dynamics of pupil and iris under variable lighting conditions, and the first integrated model in all ofthe literature to consider individual variability in pupil diameter using general equations for latency and velocity. Our image-based model for iridal pattern deformation is also the first model of its kind in the graphics literature.

9. TYPICAL REFERENCES IN NEW ACM REFERENCE FORMAT

A paginated journal article [Abril and Plant 2007], an enumerated journal article [Cohen et al. 2007], a reference to an entire issue [Cohen 1996], amonograph (whole book) [Kosiur 2001], a monograph/whole book in a series (see 2a in spec. document) [Harel 1979], a divisible-book such as an anthology or compilation [Editor 2007] followed by the same example, however we only output the series if the volume number is given [Editor 2008] (so Editor00a's series should NOT be present since it has no vol. no.), a chapter in a divisible book [Spector 1990], a chapter in a divisible book in a series [Douglass et al. 1998], a multi-volume work as book [Knuth 1997], an article in a proceedings (of a conference, symposium, workshop for example) (paginated proceedings article) [Andler 1979], a proceedings article with all possible elements [Smith 2010], an example of an enumerated proceedings article [Gundy et al. 2007], an informally published work [Harel 1978], a doctoral dissertation [Clarkson 1985], a master's thesis: [Anisi 2003], an online document / world wide web resource [Thornburg 2001], [Ablamowiczand Fauser 2007], [Poker-Edge.Com 2006], a video game (Case 1) [Obama 2008] and (Case 2) [Novak2003] and [Lee 2005] and (Case 3) a patent Scientist 2009], work accepted for publication [Rous 2008], 'YYYYb'-test for prolific author [Saeedi et al. 2010a] and [Saeedi et al. 2010b]. Other cites might contain 'duplicate' DOI and URLs (some SIAM articles) [Kirschmer and Voight 2010]. Boris / Barbara Beeton: multi-volume works as books [Hörmander 1985b] and [Hörmander 1985a].

APPENDIX

A. CLASSICAL MULTIDIMENSIONAL SCALING

Let D be an n xn matrix of pairwise distances. The matrix D is symmetric with a zero diagonal. We are interested in finding a d xn matrix X where each column x_i is the representation of the point I in R^d and$D_{ij} = \|x_i - x_j\|_2$. Denote the inner product (or Gram matrix) for this set of points by $K = X^T X$.

K is an nxn symmetric positive semidefinite matrix. Let us now abuse notation and use D^2 to indicate the matrix of squared pairwise distances $K = -1/2\ (I - 11^T)\ D^2\ (I - 11^T)$. Here, I is the n xn identity matrix and 1 is the n-vector of all ones.

ACKNOWLEDGMENTS

We are grateful to the following people for resources, discussions and suggestions: Prof. Jacobo Melamed Cattan (Ophthalmology-UFRGS), Prof. Roberto da Silva (UFRGS), Prof. Luis A. V. Carvalho (Optics-USP/SC), Prof. Anatolio Laschuk (UFRGS), Leandro Fernandes, Marcos Slomp, Leandro Lichtenfelz, Renato Silveira, Eduardo Gastal, and Denison Tavares. We also thank the volunteers who allowed us to collect pictures and videos of their irises: Alex Gimenes, Boris Starov, Christian Pagot, Claudio Menezes, Giovane Kuhn, Joao Paulo Gois, Leonardo Schmitz, Rodrigo Mendes, and Tiago Etiene.

REFERENCES

Rafal Ablamowicz and Bertfried Fauser. 2007. CLIFFORD: a Maple 11 Package for Clifford Algebra Computations, version 11. (2007). Retrieved February 28, 200 from http://math.tntech.edu/rafal/cliff11/index.html

Sten Andler. 1979. Predicate Path expressions. In *Proceedings of the 6th. ACM SIGACT-SIGPLAN symposium on Principles of Programming Languages (POPL '79)*. ACM Press, New York, NY, 226–236. DOI:http://dx.doi.org/10.1145/567752.567774

David A. Anisi. 2003. *Optimal Motion Control of a Ground Vehicle*. Master's thesis. Royal Institute of Technology (KTH), Stockholm, Sweden.

Brian Cabral and Leith C. Leedom. 1993. Imaging vector fields using line integral convolution. In *Proceedings of the 20th Annual Conference on Computer Graphics and Interactive Techniques (SIGGRAPH'93)*. ACM, New York, NY, 263–270. DOI:http://dx.doi.org/10.1145/166117.166151

Kenneth L. Clarkson. 1985. *Algorithms for Closest-Point Problems (Computational Geometry)*. Ph.D. Dissertation. Stanford University, Palo Alto, CA. UMI Order Number: AAT 8506171.

Jacques Cohen (Ed.). 1996. Special Issue: Digital Libraries. *Commun. ACM* 39, 11 (Nov. 1996).

Sarah Cohen, Werner Nutt, and Yehoshua Sagic. 2007. Deciding equivalances among conjunctive aggregate queries. *J. ACM* 54, 2, Article 5 (April 2007), 50 pages. DOI:http://dx.doi.org/10.1145/1219092.1219093

John G. Daugman. 1985. Uncertainty relation for resolution in space, spatial frequency, and orientation optimized by two dimensional visual cortical filters. *J. Optical Soc. Amer. A: Optics, Image Science, Vision* 2, 7 (1985), 1160–1169.

Bruce P. Douglass, David Harel, and Mark B. Trakhtenbrot. 1998. Statecarts in use: structured analysis and object-orientation. In *Lectures on Embedded Systems*, Grzegorz Rozenberg and Frits W. Vaandrager (Eds.). Lecture Notes in Computer Science, Vol. 1494. Springer-Verlag, London, 368–394. DOI:http://dx.doi.org/10.1007/3-540-65193-4 29

Ian Editor (Ed.). 2007. *The title of book one* (1st. ed.). The name of the series one, Vol. 9. University of Chicago Press, Chicago. DOI:http://dx.doi.org/10.1007/3-540-09237-4

Ian Editor (Ed.). 2008. *The title of book two* (2nd. ed.). University of Chicago Press, Chicago, Chapter 100. DOI:http://dx.doi.org/10.1007/3-540-09237-4

David J. Field, Anthony Hayes, and Robert F. Hess. 1993. Contour integration by the human visual system: Evidence for a local "association field". *Vision Res.* 33, 2 (1993), 173–193. DOI:http://dx.doi.org/10.1016/0042-6989(93)90156-Q

David Fowler and Colin Ware. 1989. Strokes for Representing Univariate Vector Field Maps. In *Proceedings of Graphics Interface*. Canadian Human-Computer Communications Society, Mississauga, Ontario, 249–253.

Matthew Van Gundy, Davide Balzarotti, and Giovanni Vigna. 2007. Catch me, if you can: Evading network signatures with web-based polymorphic worms. In *Proceedings of the first USENIX workshop on Offensive Technologies (WOOT '07)*. USENIXAssociation, Berkley, CA, Article 7, 9 pages.

David Harel. 1978. *LOGICS of Programs: AXIOMATICS and DESCRIPTIVE POWER*. MIT Research Lab Technical Report TR-200. Massachusetts Institute of Technology, Cambridge, MA.

David Harel. 1979. *First-Order Dynamic Logic*. Lecture Notes in Computer Science, Vol. 68. Springer-Verlag, New York, NY. DOI:http://dx.doi.org/10.1007/3-540-09237-4

Lars Hörmander. 1985a. *The analysis of linear partial differential operators. III*. Grundlehren der Mathematischen Wissenschaften [Fundamental Principles of Mathematical Sciences], Vol. 275. Springer-Verlag, Berlin, Germany. viii+525 pages. Pseudodifferential operators.

Lars Hörmander. 1985b. *The analysis of linear partial differential operators. IV*. Grundlehren der Mathematischen Wissenschaften [Fundamental Principles of Mathematical Sciences], Vol. 275. Springer-Verlag, Berlin, Germany. vii+352 pages. Fourier integral operators.

David H. Hubel and Torsten N. Wiesel. 1962. Receptive fields, binocular interaction and functional architecture in the cat's visual cortex. *J. Physiol*. 160, 1 (1962), 106–154. http://jp.physoc.org

David H. Hubel and Torsten N. Wiesel. 1968. Receptive fields and functional architecture of monkey striate cortex. (1968). http://jp.physoc.org/cgi/content/abstract/195/1/215 http://www.hubel/papers/uconn.html.

Bruno Jobard and Wilfrid Lefer. 1997. Creating evenly-spaced streamlines of arbitrary density. In Proceedings of the Eurographics Workshop. Springer Verlag, Berlin, 43–56.

Markus Kirschmer and John Voight. 2010. Algorithmic Enumeration of Ideal Classes for Quaternion Orders. *SIAM J. Comput*. 39, 5 (Jan. 2010), 1714–1747. DOI:http://dx.doi.org/10.1137/080734467

Donald E. Knuth. 1997. The Art of Computer Programming, Vol. 1: Fundamental Algorithms (3rd. ed.). Addison Wesley Longman Publishing Co., Inc.

David Kosiur. 2001. *Understanding Policy-Based Networking* (2nd. ed.). Wiley, New York, NY.

David H. Laidlaw, J. Scott Davidson, Timothy S. Miller, Marco da Silva, R. M. Kirby, William H. Warren, and Michael Tarr. 2001. Quantitative comparative evaluation of 2D vector field visualization methods. In *Proceedings of the Conference on Visualization (VIS'01)*. IEEE Computer Society, Los Alamitos, CA, 143–150.

Newton Lee. 2005. Interview with Bill Kinder: January 13, 2005. Video, *Comput. Entertain*. 3, 1, Article 4 (Jan.-March 2005). DOI:http://dx.doi.org/10.1145/1057270.1057278

Zhaoping Li. 1998. A neural model of contour integration in the primary visual cortex. *Neural Comput*. 10, 4 (1998), 903–940. DOI:http://dx.doi.org/10.1162/089976698300017557

Nick Lund. 2001. *Attention and Pattern Recognition*. Routledge, New York, NY.

Dave Novak. 2003. Solder man. Video. In *ACM SIGGRAPH 2003 Video Review on Animation theater Program: Part I – Vol. 145 (July 27–27, 2003)*. ACM Press, New York, NY, 4. DOI:http://dx.doi.org/99.9999/woot07-S422

Barack Obama. 2008. A more perfect union. Video. (5 March 2008). Retrieved March 21, 2008 from http://video.google.com/videoplay?docid=6528042696351994555

Daniel Pineo and Colin Ware. 2008. Neural modeling of flow rendering effectiveness. In *Proceedings of the5th Symposium on Applied Perception in Graphics and Visualization (APGV'08)*. ACM, New York, NY, 171–178. DOI:http://dx.doi.org/10.1145/1394281.1394313

Poker-Edge.Com. 2006. Stats and Analysis. (March 2006). Retrieved June 7, 2006 from http://www.poker-edge.com/stats.php

Bernard Rous. 2008. The Enabling of Digital Libraries. Digital Libraries 12, 3, Article 5 (July 2008). To appear.

Mehdi Saeedi, Mortez Saheb Zamani, and Mehdi Sedighi. 2010a. A library-based synthesis methodology for reversible logic. Microelectron. J. 41, 4 (April 2010), 185–194.

Mehdi Saeedi, Morteza Saheb Zamani, Mehdi Sedighi, and Zahra Sasanian.2010b. Synthesis of Reversible Circuit Using Cycle-Based Approach. *J. Emerg. Technol. Comput. Syst*. 6, 4 (Dec. 2010).

Joseph Scientist. 2009. The fountain of youth. (Aug. 2009). Patent No. 12345, Filed July 1st., 2008, Issued Aug. 9th., 2009.

Stan W. Smith. 2010. An experiment in bibliographic mark-up: Parsing metadata for XML export. In *Proceedings of the 3rd.annual workshop on Librarians and Computers (LAC '10),* Reginald N. Smythe and Alexander Noble (Eds.), Vol. 3. Paparazzi Press, Milan Italy, 422–431. DOI:http://dx.doi.org/99.9999/woot07-S422

Asad Z. Spector. 1990. Achieving application requirements. In *Distributed Systems* (2nd. ed.), Sape Mullender (Ed.). ACM Press, New York, NY, 19–33. DOI:http://dx.doi.org/10.1145/90417.90738

Harry Thornburg. 2001. Introduction to Bayesian Statistics. (March 2001). Retrieved March 2, 2005 from http://ccrma.stanford.edu/~jos/bayes/bayes.html

Greg Turk and David Banks. 1996. *Image-guided streamline placement*. Technical Report I-CA2200. University of California, Santa Barbara, CA. 453–460 pages. DOI:http://dx.doi.org/10.1145/237170.237285

Colin Ware. 2008. Toward a Perceptual Theory of Flow Visualization. *IEEE Comput. Graph. Appl*. 28, 2 (2008), 6–11. DOI:http://dx.doi.org/10.1109/MCG.2008.39

Received September 2008; accepted March 2009